J. theor. Biol. (1999) **200,** 375–388
Article No. jtbi.1999.1002, available online at http://www.idealibrary.com on IDEAL®

Simplified Dynamics of Human and Mammalian Neocortical Neurons

HUGH R. WILSON*

Visual Sciences Center, The University of Chicago, 939 East 57th Street, Chicago, IL 60637, U.S.A.

(*Received on* 21 *January* 1999, *Accepted in revised form on* 9 *July* 1999)

The behavior of human and mammalian neocortical neurons is governed by the interplay of approximately a dozen ion currents. Due to the complexity of the resulting dynamics, it is sometimes advantageous to resort to simpler systems in order to gain insight into the relationship between underlying dynamical principles and biophysics. This paper presents a new and extremely simple approximation to the dynamics of neocortical neurons based on just four simulated ion currents: I_{Na}, I_K, I_T, and I_{AHP}. The formulation incorporates Ohm's law plus explicit representation of Na^+, K^+, and Ca^{2+} equilibrium potentials, yet mathematical simplicity is retained by restriction of the dynamics to cubic nonlinearities. The resulting equations produce a good approximation to spike shapes, firing rates, and bursting behavior throughout the physiological range. Analysis of the equations suggests that four unique dynamical regimes form the basis for different categories of neocortical neurons. Synaptic coupling between these model neurons demonstrates their potential utility in simulations by producing network models of bursting and of short-term memory function.

Introduction

The elegant biophysical studies of Hodgkin & Huxley (1952) on the squid axon demonstrated that action potential generation results from an interplay of four nonlinear, time-dependent processes governing membrane potential (V), Na^+ channel activation (m), Na^+ channel inactivation (h), and K^+ channel activation (n). Subsequent investigations have shown that human and mammalian neocortical neurons are even more complex, with approximately 12 distinct ionic currents contributing to their responses (Gutnick & Crill, 1995; McCormick, 1998). Among these additional currents are a low threshold Ca^{2+} current, I_T, and a slow afterhyperpolarizing K^+ current, I_{AHP}. The diversity of neocortical spike patterns produced by these currents has been categorized into four distinct classes (Connors & Gutnick, 1990; Gutnick & Crill, 1995; Gray & McCormick, 1996). Regular spiking neurons (RS) begin firing at a high rate that decreases to a lower steady rate within approximately 100 ms (spike frequency adaptation). Fast spiking (FS) neurons typically show little or no spike frequency adaptation and also produce a briefer spike, which permits them to maintain firing rates in the 400–800 Hz range. Continuously bursting neurons (CB) and chattering cells produce a patterned spike train consisting of periodic bursts, with 2–6 spikes typically comprising each burst. Finally, intrinsic bursting cells (IB) typically begin firing with a burst of 2–6 spikes which is followed by a pause and then a transition to a tonic spike train. FS neurons are typically inhibitory, while the remaining cell

* E-mail: hrw6@midway.uchicago.edu

0022–5193/99/020375 + 14 $30.00/0

types are thought to be excitatory (McCormick *et al.*, 1985).

The diversity of neocortical ion channels and firing patterns raises two questions. First, what is the dynamical basis for this diversity? Second, do FS, RS, CB, and IB cells truly represent distinct categories, or do they represent points on a continuum of neural behaviors? Based upon neural modeling studies, Mainen & Sejnowski (1996) have suggested that the diversity of firing patterns results from separation of the fast I_{Na} and I_K currents in the axon initial segment from the slower I_T- and I_{AHP}-type currents in the soma and dendrites. They also suggested that the firing patterns of neocortical neurons might form a continuum rather than falling into discrete categories. However, the complexity of their simulation prevented them from determining whether the underlying dynamics might fall into categories defined by the nature of their singularities, presence or absence of Hopf bifurcations, etc.

The goal of this paper is to develop the simplest plausible approximation to neocortical neurons that is consistent with the observed diversity of dynamical behavior and to use this formulation to suggest answers to the questions posed above. The tradition of simplifying action potential dynamics originated with the FitzHugh–Nagumo equations (FitzHugh, 1961; Nagumo *et al.*, 1962), which comprise a two-dimensional system in V and a recovery variable R with nonlinearities limited to a cubic polynomial. Indeed, the mathematical tractability of these equations has resulted in the their continued use in neural simulations (e.g. Collins *et al.*, 1995; Longtin, 1995; Kaplan *et al.*, 1996). The model developed here retains the analytic tractability of the FitzHugh–Nagumo approach by restricting all nonlinearities to cubic polynomials. Unlike FitzHugh–Nagumo, however, the neocortical model retains the essential biophysics by explicitly incorporating Ohm's law and the appropriate equilibrium potentials in the dynamics. The resulting model consists of four differential equations simulating interactions among I_{Na}, I_K, I_T, and I_{AHP}. The model fits the observed range of neocortical responses and indicates that only four distinct categories are essential to the underlying dynamics.

Neocortical Model

The Hodgkin–Huxley (Hodgkin & Huxley, 1952) equations are based on the biophysical assumption that each ionic current must obey Ohm's law independently. It was further assumed that the effective potential for each ionic current was the difference between the membrane potential V and the equilibrium potential for the ion in question, E. With g representing the conductance, the j-th ionic current may therefore be written as

$$I_j = g_j(V - E_j). \tag{1}$$

The two ions responsible for action potential generation are Na^+ and K^+. The simplest dynamical formulation consistent with these observations is

$$C\frac{dV}{dt} = -m_\infty(V)(V - E_{Na}) - g_K R(V - E_K) + I,$$

$$\frac{dR}{dt} = \frac{1}{\tau_R}(-R + R_\infty(V)). \tag{2}$$

The first equation describes changes in the membrane potential V due to membrane capacitance (C), ionic currents, and the stimulating current I (in nA). E_{Na} and E_K are the equilibrium potentials for Na^+ and K^+, respectively, while $m_\infty(V)$ is the Na^+ activation function. The second equation describes K^+ channel activation as a function of the time constant τ_R and the equilibrium state $R_\infty(V)$. The variable in this equation has been designated R to signify that it represents a recovery variable.

Several approximations are inherent in eqn (2). As previously developed by Rinzel (1985), Na^+ activation has been assumed to be sufficiently fast to be described by its equilibrium value m_∞ (V). Second, the Na^+ conductance has no inactivation variable. This is consistent with the observation that human and mammalian neocortical neurons contain Na^+ currents that do not inactivate (Connors *et al.*, 1982; Avoli *et al.*, 1994). Several other models, such as Morris–Lecar (Morris & Lecar, 1981), also lack inactivation variables (Rinzel & Ermentrout, 1989). Third, τ_R has been chosen to be independent of V (consequences of this are discussed below).

It may be noted that eqn (2) contains no explicit representation of the leakage current. Because $m_\infty(V)$ and $R_\infty(V)$ will both be chosen to be polynomials [see eqn (3) below], however, it is possible to exactly absorb any leakage current into the linear terms of the Na^+ and K^+ currents as long as the equilibrium potential for the leakage current lies between E_{Na} and E_K. Therefore, the absence of an explicit leakage current in eqn (2) is simply a matter of mathematical convenience.

Membrane potential V has been scaled to units of mV/100 in order to keep the constants in eqn (3) within a reasonable range. Given this convention, $E_{Na} = 0.5$ and $E_K = -0.95$, corresponding to 50 and -95 mV, respectively. All plots of action potentials will be scaled by a factor of 100 for comparison with physiological data.

Restriction of eqn (2) to cubic order nonlinearities can be met if the Na^+ activation, $m_\infty(V)$, and the equilibrium state of the recovery variable, $R_\infty(V)$, are defined by quadratic functions. Appropriate forms for these functions are

$$\begin{aligned} m_\infty(V) &= 17.8 + 47.6V + 33.8V^2, \\ R_\infty(V) &= 1.24 + 3.7V + 3.2V^2. \end{aligned} \tag{3}$$

In the case of $m_\infty(V)$, a quadratic function suffices to capture the accelerating nonlinearity inherent in voltage-dependent Na^+ channel activation. Constants were chosen to provide the best fit of the dV/dt isocline [see eqn (4)] to that of the Rinzel (1985) approximation to the Hodgkin–Huxley (Hodgkin & Huxley, 1952) equations. A quadratic dependence of R was first introduced by Hindmarsh & Rose (1984) based upon their empirical model (Hindmarsh & Rose, 1982). They have argued that it represents a useful approximation to the presence of an I_A current (Rose & Hindmarsh, 1989). The mathematical relevance to the present formulation is simply that a quadratic form for $R_\infty(V)$ permits spike initiation at arbitrarily low frequencies due to a saddle-node bifurcation, which is characteristic of class-I neurons (Ermentrout, 1998). Rush & Rinzel (1994) have emphasized some of the limitations of this approximation to I_A currents.

Isoclines (i.e. nullclines) for eqns (2) and (3) are plotted in Fig. 1 and are given by

$$R = \begin{cases} \dfrac{-m_\infty(V)(V - E_{Na}) + I}{g_K(V - E_K)} & \text{for } \dfrac{dV}{dt} = 0, \\ R_\infty(V) & \text{for } \dfrac{dR}{dt} = 0. \end{cases} \tag{4}$$

The constant $g_K = 26$ here and subsequently, and this results in a -0.748 or -74.8 mV resting potential. Note that the term $(V - E_K)$ in the denominator of the first isocline equation is a consequence of Ohm's law. This means that the $dV/dt = 0$ isocline will approach infinity at $V = E_K$. Furthermore, when $I = 0$, the dV/dt isocline is zero when $V = E_{Na}$. As indicated in Fig. 1, these points on the isoclines reflect the underlying biophysics. Due to the denominator in the dV/dt isocline equation, depolarizing currents I primarily shift the left-hand dip in this isocline upward (vertical arrow in Fig. 1) without affecting the right-hand hump. This is physiologically correct and in marked contrast to the

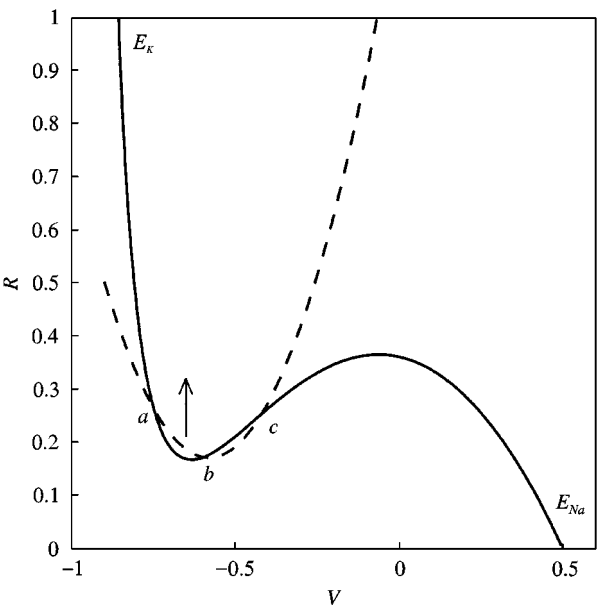

FIG. 1. Phase plane and isoclines (or nullclines) for eqns (2) and (3). The solid curve is the $dV/dt = 0$ isocline, while the dashed curve is the $dR/dt = 0$ isocline. Values of E_{Na} and E_K define the locations of the ends of the dV/dt isocline. Depolarizing currents I cause the left-hand dip in the dV/dt isocline to move upwards (arrow) causing the asymptotically stable node (a) and saddle point (b) to coalesce and vanish at a bifurcation. Beyond this saddle-node bifurcation action potentials exist as limit cycles surrounding the unstable spiral point (c).

FitzHugh–Nagumo equations. In consequence, spiking begins at a bifurcation where the saddle point (b) and node (a) disappear leaving only the unstable spiral point (c). The cubic equation for the steady states derived from eqns (3) and (4) can be solved for the current I at which the saddle-node bifurcation occurs (see the appendix). The resulting rheobase current for the model is $I = 0.178$ nA, which results in a threshold depolarization to $V = -0.68$ (i.e. -68 mV) and results in an action potential. Both rheobase and the $+7$ mV depolarization at threshold are in good agreement with data on human neurons (Foehring & Wyler, 1990). When model neurons are stimulated via appropriate synaptic currents (see below), the depolarization necessary for spike generation rises to about -0.60 (i.e. -60 mV).

As a final point elucidated by the isocline structure in Fig. 1, note that the peak height of action potentials will occur where the limit cycle crosses the dV/dt isocline on the right. However, this point is governed primarily by the Na^+ equilibrium potential E_{Na}. Reducing E_{Na} experimentally has been shown to have a dramatic effect in reducing spike height (Hodgkin & Katz, 1949), and model simulations of eqns (2) and (3) reproduce their data accurately.

To complete this simplified model for human and mammalian neocortical neurons, two further currents must be added to eqn (2). These represent approximations to a Ca^{2+} current, I_T, and a slow, Ca^{2+} mediated K^+ hyperpolarizing current, I_{AHP}. As will be emphasized in the discussion, the model I_T current lacks the inactivation characteristic of physiological I_T currents. In the spirit of the approach just developed, the resulting four-equation system is given by

$$\begin{aligned} C\frac{dV}{dt} &= -m_\infty(V-0.5) - 26R(V+0.95) \\ &\quad - g_T T(V-1.2) - g_H H(V+0.95) + I, \\ \frac{dR}{dt} &= \frac{1}{\tau_R}(-R + R_\infty(V)), \\ \frac{dT}{dt} &= \frac{1}{14}(-T + T_\infty(V)), \\ \frac{dH}{dt} &= \frac{1}{45}(-H + 3T), \end{aligned} \tag{5}$$

where T and H are the model conductance variables for I_T and I_{AHP}. As in eqn (3) for $m_\infty(V)$ and $R_\infty(V)$, cubic dynamics are maintained by restricting $T_\infty(V)$ to a quadratic polynomial

$$T_\infty(V) = 8(V + 0.725)^2. \tag{6}$$

The very small positive value of $T_\infty(V)$ at rest changes the resting potential of eqns (2) and (3) from -0.748 to -0.75, or -75 mV.

The equilibrium potentials, represented explicitly in the first equation in eqn (5), are: $E_{Na} = 0.5$ (i.e. 50 mV); $E_K = -0.95$ (i.e. -95 mV); and $E_{Ca} = 1.2$ (i.e. 120 mV). These values are similar to values adopted by others (e.g. Rush & Rinzel, 1994; Mainen & Sejnowski, 1996). Time constants are 14 ms for the dT/dt equation and 45 ms for the dH/dt equation. Finally, $C = 1.0\ \mu F\ cm^{-2}$. The remaining three parameters in eqn (5), τ_R, g_T, and g_H, will be assigned different values to simulate each distinct form of dynamical behavior observed in cortical neurons.

Derivation of the dH/dt equation deserves comment. Biophysically, H is driven by the internal Ca^{2+} concentration, which in turn depends on the Ca^{2+} current through the membrane. Representing this current exactly leads to an equation of the form

$$\frac{dH}{dt} = \frac{1}{45}(-H - kT(V - 1.2)). \tag{7}$$

Two observations permit this to be simplified to the form in eqn (5). First, the long 45 ms time constant guarantees that fluctuations in V on the time-scale of individual action potentials will be effectively invisible in eqn (7). The remaining variation in V is bounded approximately by the range $-0.8 \leqslant V \leqslant -0.6$ (see Figs 4–6). Thus, the term $(V - 1.2)$ in eqn (7) only varies by about $\pm 5\%$. Treating this term as constant produces the dH/dt equation in eqn (5). As a check on the adequacy of this constant approximation, simulations were run to compare dH/dt in eqns (5) and (7). As expected from the considerations above, the simulations did not differ significantly, and $H(t)$ computed from the two equations only varied by $\pm 5\%$. Thus, eqn (5) incorporates an approximation to eqn (7).

Regular Spiking and Fast Spiking Neurons

A major characteristic of regular spiking or RS cells is pronounced spike frequency adaptation, which can be simulated using the parameter values $g_T = 0.1$ and $g_H = 5$. In addition, the spike width of RS cells is well fit for $\tau_R = 4.2$ ms. These values produce a neuron with a pronounced I_{AHP} current and a small I_T current. The shape of RS action potentials produced by eqn (5) is compared with the measured action potential of a human RS cortical neuron (Foehring *et al.*, 1991) in Fig. 2(a). Except for small discrepancies at spike initiation and termination, the fit is quite good. In addition, the 0.9 ms spike width at half-amplitude and the peak value of 23 mV agree with data for human RS neurons averaged over several studies (McCormick, 1989; Foehring & Wyler, 1990; Foehring *et al.*, 1991; Avoli *et al.*, 1994).

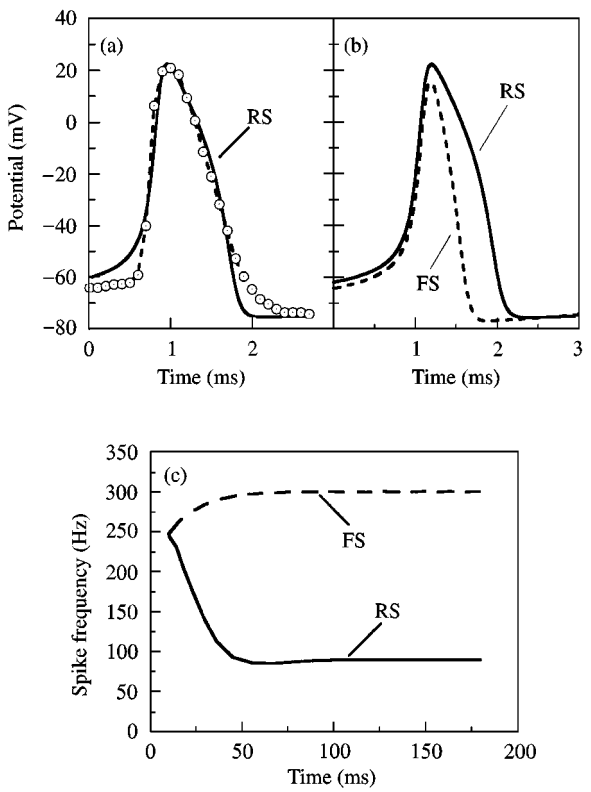

FIG. 2. Comparison of model RS and FS neurons. The model RS spike shape is compared with data from a human RS neuron (Foehring *et al.*, 1991) in (a). Reduction of τ_R from 4.2 to 1.5 ms changes the spike shape and duration from that of an RS to that of a FS neuron as shown by the comparison in (b). Instantaneous spike frequencies (reciprocals of interspike intervals) for RS and FS models are plotted in (c). Model RS cells show prominent spike frequency adaptation, while FS cells may display modest spike frequency enhancement. (---⊙---) Human.

Spike frequency (reciprocals of interspike intervals) as a function of time is plotted as a solid line in Fig. 2(c). Following onset of the 2.1 nA stimulating current, the spike rate drops by about a factor of three within 50 ms, thus exhibiting pronounced spike frequency adaptation. The approximately exponential time course of this adaptation agrees with data from both human (McCormick & Williamson, 1989; Lorenzon & Foehring, 1992) and other mammalian (Connors & Gutnick, 1990) RS neurons. The magnitude of spike frequency adaptation can be controlled by the parameter g_H in eqn (5) from none up to a point where firing ceases entirely after a finite number of spikes, which has been reported for some RS neurons (Gil & Amitai, 1996). Indeed, I_{AHP} currents have been reported to be under neuromodulatory control (McCormick & Williamson, 1989), which could easily be incorporated into eqn (5) by making g_H dependent upon the output of a modulatory control neuron.

Model RS firing rates are compared with data from human (Avoli *et al.*, 1994) and guinea pig (McCormick *et al.*, 1985) RS neurons in Fig. 3(a). Solid symbols in the figure plot the initial transient spike rates, while the open circles plot the final steady-state values of the human RS neuron. The model spike rates agree with the human transient and steady-state data, except for a modest compression of the physiological response above about 1.2 nA. Similar compression can be introduced into the model by treating τ_R in eqn (5) as a function of V rather than a constant. Even without this embellishment, however, the model spike rates fall within the physiological range for RS neurons.

While RS neurons are excitatory, inhibitory interneurons in the neocortex appear to be exclusively fast spiking or FS cells (McCormick *et al.*, 1985; Connors & Gutnick, 1990). FS neurons are characterized by much narrower action potentials, higher maximum firing rates, and little or no spike frequency adaptation. Some FS neurons even increase their firing rate by about 25% during constant current stimulation (Connors & Gutnick, 1990). Such a neuron is accurately described by eqn (5) with $g_T = 0.25$, $g_H = 0$, and

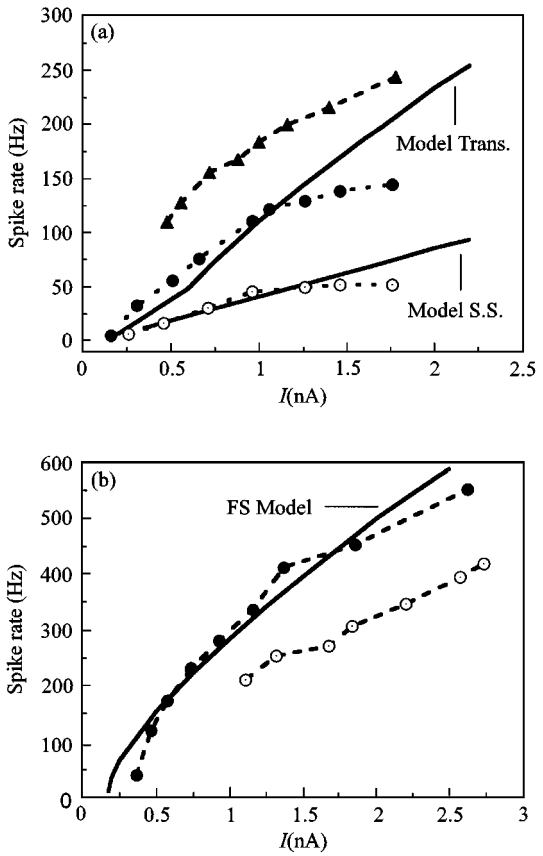

FIG. 3. Firing rates as a function of stimulus current I in nA for model RS (a) and FS (b) neurons. For the RS model in (a), both the initial transient spike rate and the final steady state (SS) are compared with data from a human RS neuron (Lorenzon & Foehring, 1992) plotted as solid and open circles. Initial transient response of a guinea pig RS neuron (McCormick *et al.*, 1985) is plotted by triangles. The response of a model FS neuron is compared with data from two guinea pig neurons (McCormick *et al.*, 1985) in (b). In agreement with physiology, the FS model produces much higher spike rates than the RS model. (··●··) human trans.; (--⊙--) human s.s.; (––▲––) G. pig trans.

$\tau_R = 1.5$ ms. The spike shape produced by this simulated FS neuron is plotted as a dashed line in Fig. 2(b). Compared to the spike of an RS neuron, the reduction of τ_R to 1.5 ms results both in a reduction of spike width to 0.5 ms and in a decrease of the spike peak to 16 mV. Both these values agree with mean human FS neuron data (Foehring *et al.*, 1991). FS neurons in other mammals have been reported to have spike widths as narrow as 0.32 ms (McCormick *et al.*, 1985; Gray & McCormick, 1996). These narrower spikes can be obtained from eqn (5) by reducing the capacitance to about $0.7\,\mu\mathrm{F\,cm^{-2}}$ and τ_R to 1.0 ms.

The spike frequency of this FS neuron in response to a 0.8 nA stimulating current is plotted as a dashed line in Fig. 2(c). The weak T-mediated current produces an increase in spike rate by about 22% during the first 50 ms of firing as shown by a subset of FS neurons (Connors & Gutnick, 1990). Initial spike rates for a model FS neuron are compared with responses of two guinea pig FS neurons (McCormick *et al.*, 1985) in Fig. 3(b), where the fit to the data plotted as black circles is certainly satisfactory. The model FS neuron can fire at rates above 600 Hz, while the model RS neuron can only produce initial firing rates up to about 275 Hz.

Continuous and Intrinsic Bursting Neurons

Continuous bursting in response to constant current stimulation has been reported for neocortical neurons in both mouse somatosensory cortex (Agmon & Connors, 1989) and cat visual cortex (Gray & McCormick, 1996), the latter having been dubbed chattering cells. These cells will be termed continuous bursting or CB neurons and will be distinguished from the intrinsic bursting (IB) neurons discussed subsequently. Equation (5) will produce a CB neuron if the parameters are set at $g_T = 2.25$, $g_H = 9.5$, and $\tau_R = 4.2$ ms. The spike train in response to a constant stimulating current $I = 0.85$ nA is plotted in Fig. 4. The response is a series of bursts at 9.0 Hz with the three spikes comprising each burst fired at 172 Hz. Notice that each burst is terminated with an after-depolarizing potential (ADP), as observed physiologically. This simply reflects the interplay between I_K, I_T, and I_{AHP}, as no explicit ADP has been incorporated into the model.

The burst rate is a monotonically increasing function of stimulus current varying from 3.6 Hz at $I = 0.2$ nA to 11.3 Hz at $I = 1.5$ nA. Over this range, the spike rate within bursts increased only modestly (from 122 to 183 Hz), and the number of spikes per burst remained constant at three (except at the lowest current level, where only two spikes comprised each burst). The decreasing spike height evident within each burst is commonly observed physiologically (Agmon & Connors, 1989; Connors & Gutnick, 1990; Gray & McCormick, 1996).

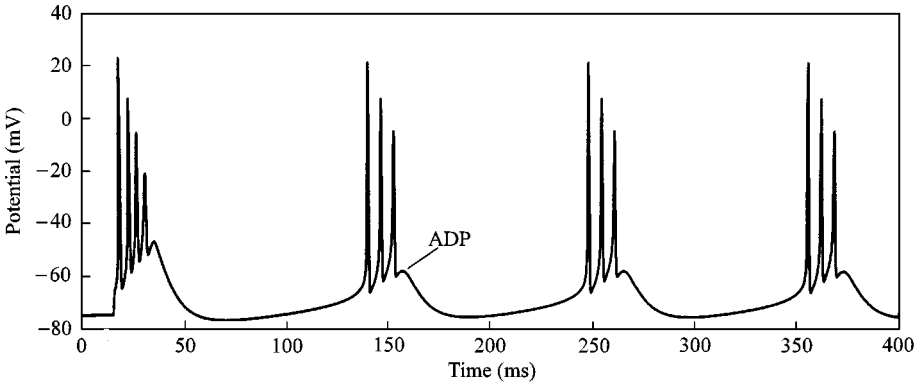

FIG. 4. Continuous bursting produced by the model in eqn (5) in response to an input current $I = 0.85$ nA. Note the after depolarizing potential (ADP) at the termination of each burst.

A mathematical analysis of this bursting behavior is straightforward. To reveal the underlying dynamics, it is convenient to simulate the application of tetrodotoxin (TTX) in order to eliminate the Na^+-mediated spikes from the response. This may be accomplished by replacing the V dependent conductance $m_\infty(V)$ in eqns (3) and (5) by its constant value at the resting potential, $V = -0.75$. This is equivalent to removing the active properties of $m_\infty(V)$ leaving only the leakage current present at rest (see the discussion of leakage currents above). The calculated value is $m_\infty(-0.75) = 1.1125$, so this value was used in the first equation of eqn (5) for TTX simulations. The 4×4 Jacobian of eqn (5) is now easily computed and has only a quadratic dependence on V (see the appendix). Application of the Routh–Hurwitz criterion (Wilson, 1999) to this Jacobian shows that a Hopf bifurcation occurs at $V = -0.6749$. Solution of the cubic equation for the steady state now shows that $I = 0.199$ nA will produce the desired value of V at equilibrium. This proves that a Hopf bifurcation, which can be shown to be supercritical, occurs in the TTX version of eqn (5) when $I = 0.199$ (see the appendix). Thus, the bursting produced by eqn (5) under normal conditions is driven by the I_T and I_{AHP} mediated limit cycle revealed under simulated TTX conditions: Ca^{2+} spikes drive the bursting. This is an example of type-II bursting (Rinzel, 1987; Bertram *et al.*, 1995). However, it is distinct from the Kopell & Ermentrout (1986) model in which slow limit cycles were required to exist under conditions where V remained constant. Limit cycles in eqn (5) under TTX conditions are mediated by the impact of I_T and I_{AHP} and V.

Instances of transient bursting are now easy to understand. As an example, intrinsic bursting or IB neurons (an apparent historical misnomer), typically fire one burst at stimulus onset, pause, and then switch to continuous firing. An example is plotted in Fig. 5 (top), for which the parameter values in eqn (5) are $g_T = 0.8$, $g_H = 4.0$, and $\tau_R = 4.2$ ms. Spikes in the initial burst here are generated at 120 Hz, while the steady firing rate following the pause in 35 Hz. Removal of the Na^+ spikes via simulated TTX application (see above) reveals that no Hopf bifurcation can occur for any value of V with these parameters. This analysis also reveals that the steady state in the TTX simulation is an asymptotically stable spiral point, which suggests that IB neural dynamics may reflect a damped oscillation mediated by the I_T and I_{AHP} currents. This is supported by the instantaneous spike rates (reciprocals of interspike intervals) plotted at the bottom of Fig. 5, where a damped oscillation in spike rate is evident.

A similar analysis provides insight into seemingly more complex transient bursting behaviors. With parameters $g_T = 1.2$, $g_H = 3.4$, and $\tau_R = 4.2$ ms, for example, eqn (5) produces the four burst transient in Fig. 6 before settling down to continuous firing. Similar physiological behavior has been reported by Connors & Gutnick [1990; Fig. 3(d)]. Again, the Jacobian under simulated TTX conditions reveals an asymptotically stable spiral point, and a damped oscillation in spike

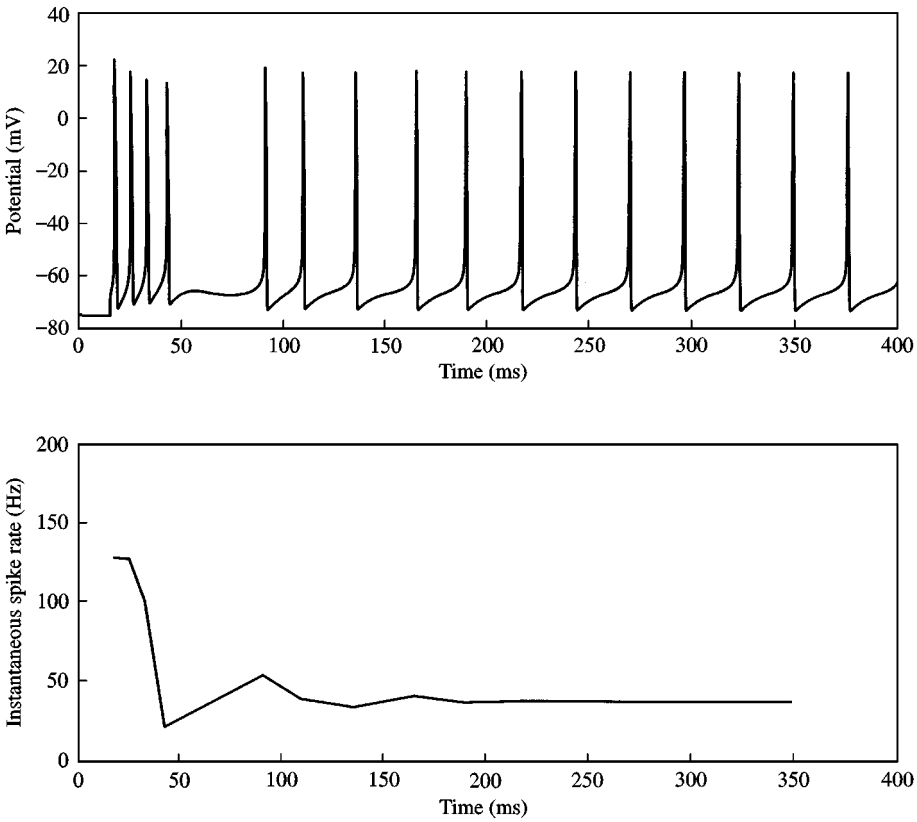

FIG. 5. Response of a model IB neuron generated by eqn (5). The top panel shows the characteristic spike train exhibiting an initial burst followed by a pause and then a transition to continuous spiking at a low rate. The lower panel shows the instantaneous spike rate (reciprocals of interspike intervals) calculated from the spike train in the top panel. Note the damped oscillation apparent in this plot.

rate consistent with this is shown by the plot at the bottom of Fig. 6.

Synaptic Connections

The simplified cortical neuron model developed above was designed to be used in network simulations. To accomplish this it is necessary to introduce synaptic interconnections among multiple model neurons. A simple way to do this is through a differential equation formulation of Rall's (1967, 1989) alpha function. This requires adding the following two equations to the four in eqn (5):

$$\frac{df}{dt} = \frac{1}{\tau_{syn}}(-f + Hvs(V_{pre} - \Omega)),$$

$$\frac{dS}{dt} = \frac{1}{\tau_{syn}}(-S + f), \tag{8}$$

where

$$Hvs(V_{pre} - \Omega) = \begin{cases} 1 & \text{if } V_{pre} - \Omega > 0, \\ 0 & \text{if } V_{pre} - \Omega \leqslant 0. \end{cases}$$

V_{pre} is the membrane potential of the pre-synaptic neuron, Ω is the threshold for a synaptic conducatance change, and Hvs is the Heaviside step function. With $\Omega = -0.1$ (i.e. -10 mV), the equations for f and S are only activated during the peak of the pre-synaptic spike. The effect of S on the membrane potential V of the post-synaptic neuron is given through addition of the term

$$-g_{syn}S(V - E_{syn})$$

to the dV/dt equation in eqn (5). E_{syn} is the synaptic reversal potential, which would typically be 0 mV for excitatory synapses and -0.75 to

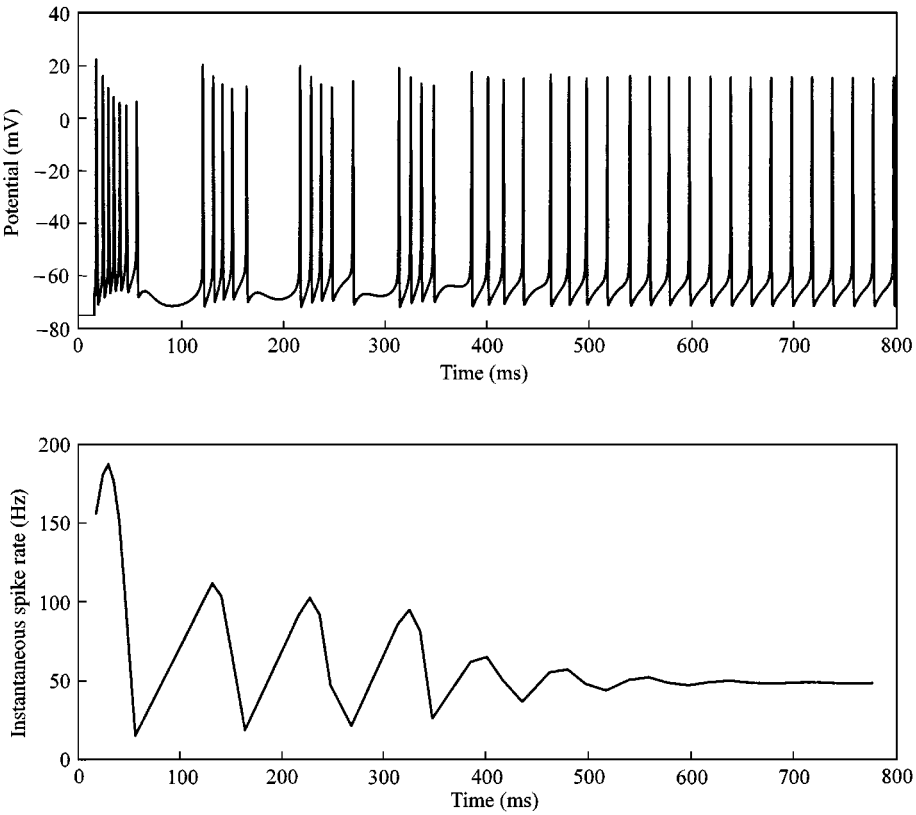

FIG. 6. A more complex example of four transient bursts followed by a transition to continuous spiking. The spike train is shown in the top panel, while the instantaneous spike rate is plotted below. The damped oscillation driving the spiking behavior is clearly revealed by the instantaneous spike rate plot.

-0.95 (-75 to -95 mV) for $GABA_a$ and $GABA_b$ inhibitory synapses.

To demonstrate that this formulation generates interesting network properties, let us consider one of the simplest scenarios: two RS neurons reciprocally connected by excitatory synapses. It was found that $g_{syn} = 20$ with $\tau_{syn} =$ 2 ms was sufficient to ensure that a single presynaptic spike could trigger a spike in the postsynaptic neuron. Using the standard parameter values for model RS cells, $g_T = 0.1$ and $g_H = 5$, one of the two interconnected neurons was continuously stimulated with an input current $I = 0.5$ nA. As shown in Fig. 7, this led to repeated bursting by the two neurons rather than the simple spike frequency adaptation produced in the absence of synaptic interactions. The bursting results from recurrent excitation causing the model neurons to fire at a rate high enough to produce a potent I_{AHP} current that temporarily arrests spiking. In addition to intrinsically generated bursting in CB or chattering neurons, this simulation demonstrates that bursting can also be produced by a very simple network of interacting RS neurons with spike frequency adaptation.

McCormick & Williamson (1989) have demonstrated that spike frequency adaptation caused by I_{AHP} currents is under neuromodulatory control. To mimic neuromodulation, let us set $g_H = 0.4$, thereby greatly reducing spike frequency adaptation. Again consider two reciprocally excitatory RS neurons with all other parameters identical to those used in the previous network simulation. If one neuron is now stimulated for just 10 ms with $I = 0.5$ nA, the two neurons generate the firing pattern shown in Fig. 8. Recurrent excitation switches the two neurons into a short-term memory state in which they continue to fire at rates of 150–200 Hz for over 320 ms after stimulus termination. Finally, build-up of the weak I_{AHP} current shuts off the recurrent activity. Thus, neuromodulation of reciprocally coupled

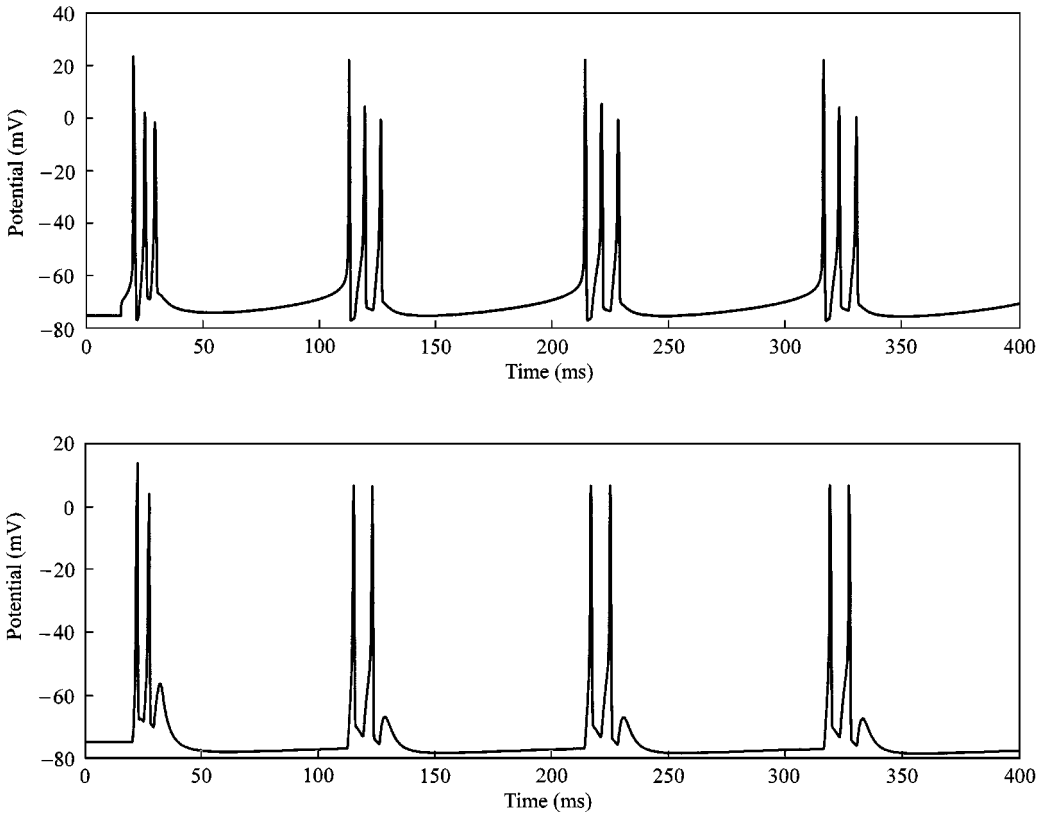

FIG. 7. Responses of two reciprocally excitatory RS neurons in response to continuous stimulation of the top neuron with $I = 0.5$ nA. Bursting reflects an interplay between recurrent excitation and strong spike frequency adaptation driven by I_{AHP} currents.

RS neurons can produce a self-terminating short-term memory store, which might be useful, for example, in converting temporal patterns into spatial patterns in auditory cortex.

Discussion

The simplified model for neocortical neuron dynamics embodied in eqn (5) has been shown to produce the range of dynamical behaviors reported for RS, FS, CB, and IB neurons. The essential dynamical components of the model are: observance of Ohm's law, cubic dynamics, and incorporation of four currents. Ohm's law coupled with cubic dynamics suffices to produce accurate spike shapes and firing rates. Of the four currents, the two faster ones (I_{Na} and I_K) are responsible for spike generation via saddle-node bifurcation to a limit cycle, while the slower two (I_T and I_{AHP}) modulate firing to produce spike frequency adaptation and bursting.

Mainen & Sejnowski (1996) have shown that a wide range of cortical firing patterns can be reproduced by the two-compartment Pinsky–Rinzel (Pinsky & Rinzel, 1994) model. In this model the spike generating I_{Na} and I_K currents are located in the soma, while remaining currents including I_T and I_{AHP} were relegated to the dendritic compartment. A variety of dynamic firing behaviors, including bursting, was then produced by varying the coupling between compartments. Based on their simulations, Mainen & Sejnowski (1996) suggest that there is a continuum of neocortical firing behaviors. The model in eqn (5), for which a detailed mathematical analysis is possible, suggests an alternative. First, although separation of fast and slow currents into separate compartments may be sufficient for generating a range of neocortical dynamics, the fact that eqn (5) describes an isopotential model indicates that two compartments are not necessary. Neocortical dynamics may be contrasted with the case of

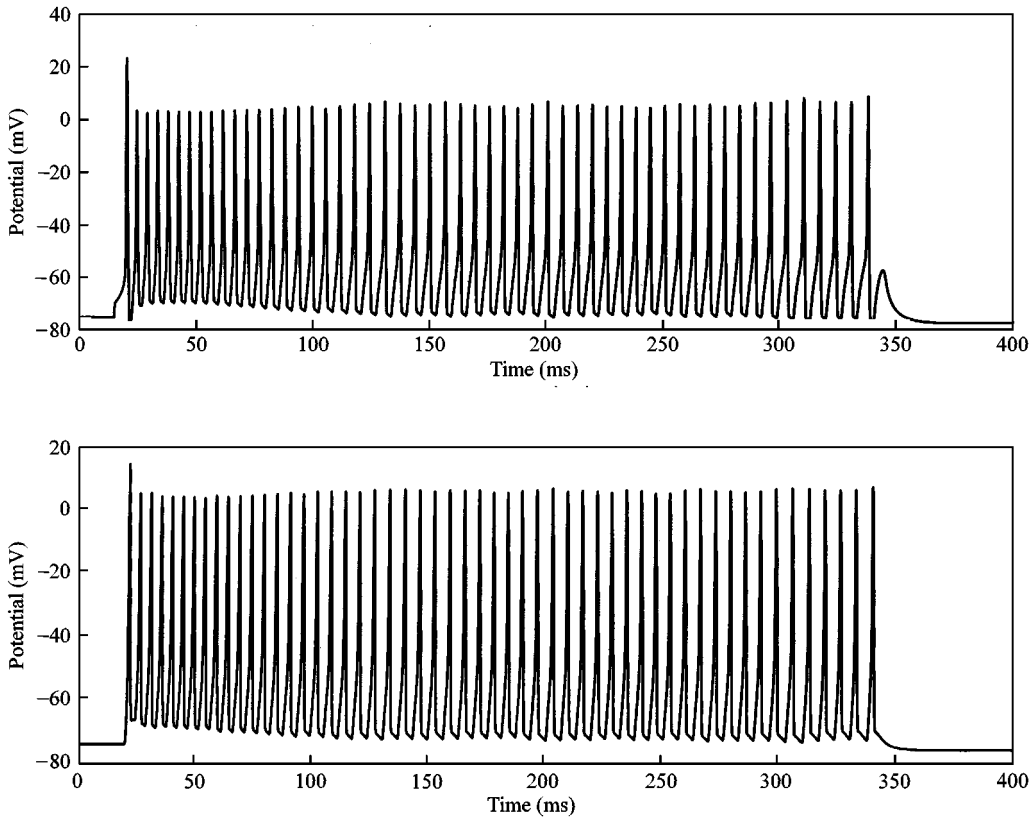

FIG. 8. Responses of two reciprocally excitatory RS neurons with greatly attenuated g_H resulting from simulated neuromodulation. In response to a 10 ms pulse to the neuron in the top panel, excitatory synaptic coupling produces spike trains that outlast the stimulus by approximately 320 ms. This short-term memory is finally terminated by the slow build-up of weak I_{AHP} currents.

plateau potentials in motorneurons, where Booth & Rinzel (1995) have demonstrated that separation of slow and fast currents into separate compartments is indeed essential.

A more important consequence of the model developed here is the demonstration that the range of neocortical firing patterns can be captured by a few discrete underlying dynamical regimes. Both RS and FS neurons are characterized by a saddle-node bifurcation to firing. When $g_T \approx 0.1$ and $g_H > 0$, spike frequency adaptation characteristic of RS cells is produced, while $g_T \geqslant 0$ and $g_H \approx 0$ produces a model FS neuron with slight frequency enhancement (when $g_T > 0$). Setting $\tau_R = 4.2$ ms for RS neurons and $\tau_R = 1.5$ ms for FS neurons does not qualitatively affect the dynamics but instead serves to provide reasonably accurate fits to the spike shapes and peak amplitudes of these two cell types. In this context, it is worth noting that the Mainen & Sejnowski (1996) two-compartment model cannot reproduce these differences in spike shapes. Continuous bursting is produced by eqn (5) under conditions where elimination of the active Na^+ current via simulated TTX application results in a dynamical regime exhibiting a supercritical Hopf bifurcation to I_T- and I_{AHP}-mediated limit cycles. Typical parameter ranges for these CB neurons are $g_T > 2.2$ and $g_H > 8$, with different burst patterns (e.g. differing numbers of spikes per burst) occurring for different parameter ranges. Finally, IB neurons may be simulated by an intermediate range of parameter values that suffice to produce an asymptotically stable spiral point under simulated TTX conditions, typical parameter ranges being $1.4 > g_T > 0.7$ and $5 > g_H > 3$ (approximate ranges). The damped oscillation is apparent in plots of instantaneous spike frequency for model IB dynamics (Figs 5 and 6), and similar plots of

experimental data might be used to produce evidence for damped oscillations under physiological conditions. Thus, analysis of the simplified dynamical model in eqn (5) indicates that the spectrum of neocortical spike patterns can be reproduced based on just four discrete underlying dynamical regimes.

With the exception of g_T, g_H, and τ_R, all parameters in eqn (5) have been kept constant in order to emphasize the relationships among dynamical modes producing different firing behaviors. Obviously, however, the model can be improved in particular instances by adjusting other parameters. For example, decreasing the time constants of the T and H equations by about a factor of 3.0 greatly increases burst frequencies, thereby providing a much better fit to the bursting of chattering cells (Gray & McCormick, 1996). Even the unusual spike shapes produced by cardiac Purkinje fibers (Noble, 1985) can be fit with the cubic dynamics in eqn (5) along with suitable parameter values.

One approximation inherent in the model is that neither I_{Na} nor I_T incorporates an inactivation variable, although both currents do inactivate biophysically. (The Morris–Lecar (Morris & Lecar, 1981) equation also lacks an inactivation variable for I_{Na}.) In the model, these currents are terminated by the hyperpolarizing currents I_K and I_{AHP}. This approach is necessary to retain cubic dynamics in eqn (5). If one were to incorporate explicit inactivation, the dynamics would perforce be described by fifth-order polynomial nonlinearities, thus giving rise to the possibility of five equilibrium states. Rush & Rinzel (1994) have explored a thalamic neuron model in which inactivation of an I_T current does produce five steady states, and that behavior cannot be replicated by eqn (5) without explicit I_T inactivation. However, the cubic dynamics in eqn (5) do suffice to reproduce a wide range of neocortical firing patterns.

The cubic dynamical model developed here may be contrasted with several other models in the literature. The FitzHugh (1961), Nagumo *et al.* (1962), and Hindmarsh–Rose (Hindmarsh & Rose, 1984) equations, although also cubic, lack the essential biophysics incorporated into eqn (5) through adherence to Ohm's law and explicit representation of the equilibrium potentials for Na^+, K^+, and Ca^{2+}. In consequence, none of these models produces accurate spike shapes or firing rates. Because eqn (5) is as analytically tractable and computationally efficient as these other equations, it should be preferable for biophysically plausible simulations. The model embodied in eqn (5) cannot, of course, produce the same level of accuracy as biophysical models that explicitly incorporate a dozen currents identified in neocortical neurons. For example, it cannot reproduce voltage clamp data accurately because of the lack of I_{Na} and I_T inactivation variables. Furthermore, it will not produce post-inhibitory rebound firing with the parameters discussed here, although somewhat modified parameters do make this possible (Wilson, 1999). Thus, the cubic dynamical model developed here is intended as a major improvement over the FitzHugh–Nagumo and Hindmarsh–Rose models rather than as an alternative to much more elaborate and computationally intensive biophysical models.

The model in eqn (5) may also be compared with "integrate and fire" models. However, those models are no more computationally efficient than eqn (5), and they make no attempt to describe action potential shapes. In addition, integrate and fire models have difficulty simulating neocortical bursting, which is driven by underlying limit cycle dynamics.

The four equation model developed here should be useful for simulations of neocortical function in preference to less realistic models such as FitzHugh–Nagumo or Hindmarsh–Rose. Indeed, the simulations of two interacting RS neurons in Figs 7 and 8 demonstrate the utility of the approach based on eqn (5). Finally, the analytic tractability of the model can enable one to reveal the dynamical basis of network properties, such as the propagation of synchronized bursting waves in slow wave sleep (Wilson, 1999).

This research was supported in part by NIH grant no. EY02158. Critiques by two anonymous referees led to great improvements in this paper.

REFERENCES

AGMON, A. & CONNORS, B. W. (1989). Repetitive burst-firing neurons in the deep layers of mouse somatosensory cortex. *Neurosci. Lett.* **99,** 137–141.

AVOLI, M., HWA, G. G. C., LACAILLE, J.-C., OLIVIER, A. & VILLEMURE, J.-G. (1994). Electrophysiological and repetitive firing properties of neurons in the superficial/middle layers of the human neocortex maintained *in vitro*. *Exp. Brain Res.* **98,** 135–144.

BERTRAM, R., BUTTE, M. J., KIEMEL, T. & SHERMAN, A. (1995). Topological and phenomenological classification of bursting oscillations. *Bull. Math. Biol.* **57,** 413–439.

BOOTH, V. & RINZEL, J. (1995). A minimal, compartmental model for a dendritic origin of bistability in motoneuron firing patterns. *J. Comput. Neurosci.* **2,** 299–312.

COLLINS, J. J., CHOW, C. C. & IMHOFF, T. T. (1995). Stochastic resonance without tuning. *Nature* **376,** 236–238.

CONNORS, B. W. & GUTNICK, M. J. (1990). Intrinsic firing patterns of diverse neocortical neurons. *TINS*, **13,** 99–104.

CONNORS, B. W., GUTNICK, M. J. & PRINCE, D. A. (1982). Electrophysiological properties of neocortical neurons *in vitro*. *J. Neurophysiol.* **48,** 1302–1320.

ERMENTROUT, B. (1998). Neural networks as spatio-temporal pattern-forming systems. *Rep. Prog. Phys.* **61,** 353–430.

FITZHUGH, R. (1961). Impulses and physiological states in models of nerve membrane. *Biophys. J.* **1,** 445–466.

FOEHRING, R. C., LORENZON, N. M., HERRON, P. & WILSON, C. J. (1991). Correlation of physiologically and morphologically identified neuronal types in human association cortex *in vitro*. *J. Neurophysiol.* **66,** 1825–1837.

FOEHRING, R. C. & WYLER, A. R. (1990). Two patterns of firing in human neocortical neurons. *Neurosci. Lett.* **110,** 279–285.

GIL, Z. & AMITAI, Y. (1996). Properties of convergent thalamocortical and intracortical synaptic potentials in single neurons of neocortex. *J. Neurosci.* **16,** 6567–6578.

GRAY, C. M. & MCCORMICK, D. A. (1996). Chattering cells: superficial pyramidal neurons contributing to the generation of synchronous oscillations in the visual cortex. *Science* **274,** 109–113.

GUTNICK, M. J. & CRILL, W. E. (1995). The cortical neuron as an electrophysiological unit. In: *The Cortical Neuron* (Gutnick, M. J. & Moody, I., eds), pp. 33–51. New York: Oxford University Press.

HINDMARSH, J. L. & ROSE, R. M. (1982). A model of the nerve impulse using two first-order differential equations. *Nature* **296,** 162–164.

HINDMARSH, J. L. & ROSE, R. M. (1984). A model of neuronal bursting using three coupled first order differential equations. *Proc. R. Soc. Lond. B* **221,** 87–102.

HODGKIN, A. L. & HUXLEY, A. F. (1952). A quantitative descritption of membrane current and its application to conduction and excitation in nerve. *J. Physiol.* **117,** 500–544.

HODGKIN, A. L. & KATZ, B. (1949). The effect of sodium ions on the electrical activity of the giant axon of the squid. *J. Physiol.* **108,** 37–77.

KAPLAN, D. T., CLAY, J. R., MANNING, T., GLASS, L., GUEVARA, M. R. & SHRIER, A. (1996). Subthreshold dynamics in periodically stimulated squid giant axons. *Phys. Rev. Lett.* **76,** 4074–4077.

LONGTIN, A. (1995). Synchronization of the stochastic Fitzhugh–Nagumo equations to periodic forcing. *II Nuovo Cimento* **17,** 835–846.

LORENZON, N. M. & FOEHRING, R. C. (1992). Relationship between repetitive firing and afterhyperpolarizations in human neocortical neurons. *J. Neurophysiol.* **67,** 350–363.

MAINEN, Z. F. & SEJNOWSKI, T. J. (1996). Influence of dendritic structure on firing pattern in model neocortical neurons. *Nature* **382,** 363–366.

MCCORMICK, D. A. (1989). GABA as an inhibitory neurotransmitter in human cerebral cortex. *J. Neurophysiol.* **62,** 1018–1027.

MCCORMICK, D. A. (1998). Membrane properties and neurotransmitter actions. In: *The Synaptic Organization of the Brain*, Shepherd G. M., ed.), pp. 37–75. New York: Oxford University Press.

MCCORMICK, D. A., CONNORS, B. W., LIGHTHALL, J. W. & PRINCE, D. A. (1985). Comparative electrophysiology of pyramidal and sparsely spiny stellate neurons of the neocortex. *J. Neurophysiol.* **54,** 782–806.

MCCORMICK, D. A. & WILLIAMSON, A. (1989). Convergence and divergence of neurotransmitter action in human cerebral cortex. *Proc. Nat. Acad. Sci.* **86,** 8098–8102.

MORRIS, C. & LECAR, H. (1981). Voltage oscillations in the barnacle giant muscle fiber. *Biophys. J.* **35,** 193–213.

NAGUMO, J. S., ARIMOTO, S. & YOSHIZAWA, S. (1962). An active pulse transmission line simulating a nerve axon. *Proc. IRE* **50,** 2061–2070.

NOBLE, D. (1985). Ionic mechanisms in rhythmic firing of heart and nerve. *TINS* **8,** 499–504.

PINSKY, P. F. & RINZEL, J. (1994). Intrinsic and network rhythmogenesis in a reduced Traub model for CA3 neurons. *J. Comput. Neurosci.* **1,** 39–60.

RALL, W. (1967). Distinguishing theoretical synaptic potentials computed for different soma-dendritic distributions of synaptic inputs. *J. Neurophys.* **30,** 1138–1168.

RALL, W. (1989). Cable theory for dendritic neurons. In: *Methods in Neuronal Modeling: from Synapses to Networks.* (Koch, C. & Segev, I. eds), pp. 9–62. Cambridge, MA: MIT Press.

RINZEL, J. (1985). Excitation dynamics: insights from simplified membrane models. *Fed. Proc.* **44,** 2944–2946.

RINZEL, J. (1987). A formal classification of bursting mechanisms in excitable systems. In: *Mathematical Topics in Population Biology, Morphogenesis, and Neurosciences*, (Teramoto, E. & Yamaguti, M., eds), pp. 267–281. Berlin: Springer.

RINZEL, J. & ERMENTROUT, G. B. (1989). Analysis of neural excitability and oscillations. In: *Methods in Neuronal Modelling: from Synapses to Networks*, (Koch, C. & Segev, I., eds), pp. 135–169. Cambridge, MA: MIT Press.

ROSE, R. M. & HINDMARSH, J. L. (1989). The assembly of ionic currents in a thalamic neuron, I. The three-dimensional model. *Proc. R. Soc. Lond. B* **237,** 267–288.

RUSH, M. E. & RINZEL, J. (1994). Analysis of bursting in a thalamic neuron model. *Biol. Cybernet.* **71,** 281–291.

WILSON, H. R. (1999). *Spikes, Decisions & Actions: Dynamical Foundations of Neuroscience.* Oxford: Oxford University Press.

APPENDIX

This appendix lists the steady-state equation and the Jacobian for the model in eqn (5). Equilibrium points of the model are given by the

following equation under normal conditions:

$$I = (8g_T + 24g_H + 117)V^3 + \tfrac{1}{50}(100g_T + 2880g_H + 10297)V^2 + \tfrac{1}{100}(-971.5g_T + 4567.5g_H + 11763)V - 5.046g_T + 11.984g_H + 21.728.$$

As the equation is cubic, there must be either one or three real roots, the latter case occurring when $g_T = g_H = 0$. For parameter values describing CB neurons only one real root occurs. Under simulated TTX conditions, the equation for equilibria becomes

$$I = \tfrac{8}{5}(5g_T + 15g_H + 52)V^3 + \tfrac{1}{25}(50g_T + 1440g_H + 4381)V^2 + \tfrac{1}{200}(-1943g_T + 9135g_H + 24948)V - 5.046g_T + 11.984g_H + 30.072.$$

The Jacobian associated with eqn (5) is given by

$$\mathbf{A} = \begin{pmatrix} F(V) & -26(V+0.95) & -g_T(V-1.2) & -g_H(V+0.95) \\ \frac{1}{\tau_R}(6.4V + 3.7) & -\frac{1}{\tau_R} & 0 & 0 \\ \frac{8}{7}(V + 0.725) & 0 & -\frac{1}{14} & 0 \\ 0 & 0 & \frac{1}{15} & -\frac{1}{45} \end{pmatrix}.$$

When $g_T = g_H = 0$, only the upper-left quadrant of the matrix is relevant. The function $F(V)$ in the upper-left of the matrix has different forms for normal and simulated TTX conditions. For normal and TTX conditions, these are respectively,

$$F(V) = -\tfrac{1}{5}(40g_T + 120g_H + 923)V^2 - \tfrac{2}{5}(29g_T + 87g_H + 394)V - 4.205g_T - 12.615g_H - 26.24,$$

$$F(V) = -\tfrac{8}{5}(5g_T + 15g_H + 52)V^2 - \tfrac{1}{5}(58g_T + 174g_H + 481)V - 4.205g_T - 12.615g_H - 33.352.$$

For any values of g_T and g_H, the Jacobian can be used in conjunction with the appropriate form of $F(V)$ to determine whether there is a value of V at which a Hopf bifurcation occurs. This may be done using the Routh–Hurwitz criterion for a pair of pure imaginary eigenvalues of the Jacobian (see Wilson, 1999). Finally, this value of V may be substituted into the steady-state equation to determine the stimulating current I at which the bifurcation occurs.